

Prediction of Aerodynamic Coefficients for Multi-Swept Delta Wings via a Neural Network

Moritz Zieher^{*†} and Christian Breitsamter^{*}

^{*}Chair of Aerodynamics and Fluid Mechanics, Technical University of Munich
Boltzmannstr. 15, 85748 Garching bei München, Germany

moritz.zieher@tum.de

[†]Corresponding author

Abstract

In this study, the prediction capabilities of a hybrid neural network with regards to aerodynamic coefficients of multiple swept delta wings are investigated. The quick evaluation of aerodynamic coefficients based on a few geometrical and flow parameters instead of cost-consuming computational fluid dynamics simulations or wind tunnel experiments could save time and costs during early aircraft design phases. The training data is based on the results of wind tunnel measurements for a number of multiple swept delta wing configurations with varying leading-edge sweeps. These datasets contain angle of attack slopes for the basic configurations, as well as measurements with deflected control surfaces and an applied sideslip angle. The results show, that different aerodynamic coefficients can be predicted accurately by machine learning models. The neural network shows great abilities in forecasting the aerodynamic characteristics and trends in coefficient slopes. Producing highly accurate predictions with respect to lift coefficients and its derivative, the prediction accuracy can vary for the pitching moment coefficient, mispredicting absolute values while still matching slope trends very well.

1. Introduction and Motivation

High-agility, high-performance aircraft configurations often show opposite aerodynamic challenges along their flight envelope. Being designed for supersonic cruise, such configurations are also required to perform high-agility maneuvers at trans- and subsonic speeds. Low-speed performance demands high lift, which further leads to the need of high angles of attack. To fulfill these requirements such aircraft configurations often consist of low-aspect-ratio wings with medium to high leading-edge sweep angles to exploit flow structures such as separated flows, leading-edge vortex systems and vortex-to-vortex or vortex-to-shock interactions [1]. Numerous experimental and numerical studies have been performed to gain an in-depth understanding of these flow features [2, 3, 4]. Polhamus reviews aerodynamic research on slender wing benefits and summarizes vortex flow technologies useful for future aircraft [5]. Further, Breitsamter presents investigations on turbulent flow fields and unsteady surface pressures caused by leading-edge vortices based on wind tunnel experiments [6].

Just the possible combinations of angles of attack, angles of sideslip and control surface deflections at a distinct Mach number call for an enormous amount of computational fluid dynamics simulations in the aircraft design phase.

Increasing computational power has led to the exploration of machine-learning techniques for fluid mechanics and aerodynamics. Enormous amounts of existing data from experiments and numerical simulations can be used to understand flow physics better and adopt or improve existing or develop computational models solely based on data [7]. In their review, LeCun et al. state, that deep learning beats other machine learning techniques in speech and visual object recognition, object detection and other domains such as drug discovery and genomics. Additionally, deep learning requires minimal engineering by hand, so it can easily take advantage of available data [8].

Zhang et al. developed a convolutional neural network (CNN) to predict the lift coefficient of differently shaped airfoils based on variable flow conditions and an objective geometry [9]. The resulting CNN shows comparable learning capabilities to a multi-layer perceptron (MLP), while exhibiting minimal constraints in geometric representation. The use of a recurrent neural network for predicting lift coefficients at high angles of attack, with special emphasis on dynamic stall identification of rotor blades at high speeds, is described by Suresh et al. [10]. Nørgaard et al. investigate the possibility of reducing wind-tunnel test times by employing a hybrid neural network optimization method [11]. A new non-iterative training algorithm for neural networks to interpolate and extrapolate data from only a few experiments

PREDICTION OF AERODYNAMIC COEFFICIENTS

and/or CFD computations is implemented by Meade et al. [12]. Using an artificial neural network, Huang et al. investigated a multi-point inverse airfoil design method, where results show reasonable accuracy for lift and pitching moment coefficient predictions [13]. Recently, Stradtner et al. published the work summary of the NATO/STO research task group AVT-351 [14]. The group explores the application of reduced order modeling techniques for time-dependent manoeuvre prediction and data set population, where roughly a third of the proposed techniques are neural network approaches. By applying a wide range of methods of reduced order modeling to different use cases, they can identify the strengths and weaknesses of the approaches for specific applications. Hines Chaves et al. work on data-driven reduced order modeling for aerodynamic flow predictions [15]. They show the capabilities of three different deep learning techniques compared to state-of-the-art reduced order modeling techniques with an additional outline of future techniques which will take spatial correlations of aerodynamic flow topologies into account.

This study investigates the prediction capabilities concerning integral aerodynamic coefficients of a hybrid neural network consisting of a conventional feed-forward neural network and a convolutional neural network. The results of wind-tunnel experiments of multiple swept delta wing configurations with sharp leading-edges serve as training data for the neural network. To cut cost and time in the preliminary aircraft design phase, this prediction tool could help to identify promising aircraft configurations regarding the aerodynamic coefficient slopes and derivatives.

2. Test Cases: Multiple Swept Delta Wings

Within this section, the generic high-agility aircraft configurations are introduced. Essential geometrical properties and the available experimental datasets are briefly described. The last part of the section provides a summary of data acquisition.

2.1 Generic Planforms

In this study, generic wing-fuselage configurations in the form of triple (NA1 W1) and double (NA1 W2) delta wing configurations with varying leading-edge sweep angles are considered. The wind tunnel models consist of a fuselage and interchangeable flat plate wings with sharp leading-edges. Additionally, each configuration type is equipped with deflectable control surfaces, e.g. levcons for triple delta wings and slats for double and triple delta wings.

These geometries were and are subject to a common research program in cooperation with Airbus Defence and Space and the German Aerospace Center and are further embedded in the NATO AVT-316 task group [16]. Various experimental and numerical studies have been performed for a range of configurations [17, 18, 19, 20, 21, 22]. In Table 1, the most important geometrical parameters of the two configuration types are listed. Additionally, an overview of the two different types are depicted in Figures 1 and 2.

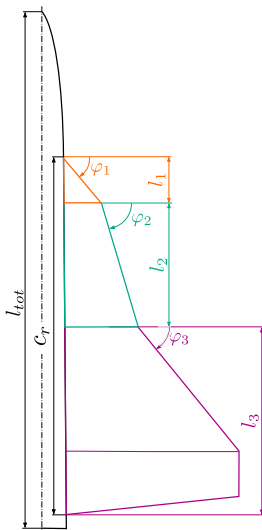


Figure 1: NA1 W1

Table 1: Geometrical properties for the generic triple and double delta wing configurations.

	NA1 W1	NA1 W2
c_r [m]	0.65 – 0.83	0.58 – 0.8
s [m]	0.32 – 0.53	0.29 – 0.468
S_{ref} [m ²]	0.29 – 0.43	0.25 – 0.35
Λ [–]	1.4 – 2.74	1.34 – 2.62
l_{tot} [m]	1.16	1.16
l_{μ} [m]	0.44 – 0.565	0.395 – 0.54
l_1/c_r [–]	–	0.125
l_2/c_r [–]	0.25/0.35	0.375/0.475
l_3/c_r [–]	0.35	0.35
φ_1 [°]	45 – 60	–
φ_2 [°]	70 – 75	70 – 75
φ_3 [°]	45 – 60	45 – 60

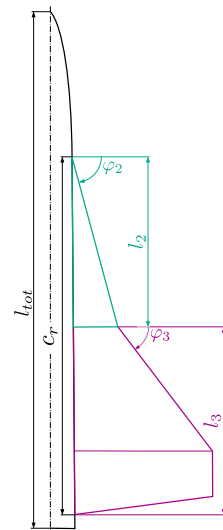


Figure 2: NA1 W2

2.2 Experimental Datasets

For this study a set of 21 different configurations at a Mach number of $M_\infty = 0.15$ is considered. In Table 2, the available combinations of angle of attack α , angle of sideslip β as well as the control surface deflections η_{levcon} and ε_{slats} are listed. For each considered configuration, there exist at least four distinct datasets in the angle of attack range of $\alpha = 0^\circ - 40^\circ$.

Table 2: Available datasets per configuration with respect to angle of attack α , angle of sideslip β and control surface deflections η_{levcon} and ε_{slats} . All datasets refer to a Mach number of $M_\infty = 0.15$.

	NA1 W1	NA1 W2
α [$^\circ$]	0 – 40	0 – 40
β [$^\circ$]	0/5	0/5
η_{levcon} [$^\circ$]	–	0/15/30
ε_{slats} [$^\circ$]	0/22.5	0/22.5

2.3 Data Acquisition

The datasets used in this study are the results of experiments by Pfnür et al., which were conducted in the course of a common research program of Airbus Defence and Space (Airbus DS), the German Aerospace Center (DLR) and the Technical University of Munich (TUM) [17, 18]. Moreover, the geometries are embedded in the NATO AVT-316 task group, where two distinct configuration types are investigated in detail [16, 19, 21, 22].

The experiments have been carried out in the Göttingen-type low-speed wind tunnel (W/T) A at the Chair of Aerodynamics and Fluid Mechanics of TUM, featuring a test section size of $1.8 \text{ m} \times 2.4 \text{ m} \times 4.8 \text{ m}$ (height \times width \times length). Aerodynamic forces and moments were acquired by an internal six-component strain-gauge balance with a sampling frequency of $f_{meas} = 800 \text{ Hz}$ over the period of $t_{meas} = 10 \text{ s}$. Pfnür et al. additionally provided repeatability measurements of the applied test setup, where their results showed $\Delta C_D = \pm 0.0035$, $\Delta C_L = \pm 0.0051$, $\Delta C_m = \pm 0.0017$ and $\Delta C_l = \pm 0.0005$ [17, 18].

In Figure 3, the setup of the wind tunnel models, for which the results will be discussed in section 4, are depicted.



Figure 3: Experimental setup of the wind tunnel models.

3. Prediction Model

In the following section, a detailed introduction of the proposed hybrid neural network (HNN) is given. In the second part, the applied process of hyperparameter optimization is described. Necessary preprocessing steps are briefly outlined in the third part of the section, followed by the network training process. The definition of error and performance quantification of the trained HNN concludes this section.

3.1 Hybrid Neural Network

Hybrid neural networks are combinations of conventional neural network architectures, described e.g. by Yuan et al., and can be used to combine the benefits of convolutional neural networks (CNN) with additional inputs by a multi-layer

PREDICTION OF AERODYNAMIC COEFFICIENTS

perceptron (MLP) [23, 24].

In Figure 4, the architecture of the HNN is depicted. The well-known image recognition capability of a CNN architecture is used to identify the current aircraft configuration [25]. After the propagation through a number of convolutional layers, the compromised geometry information is combined with experimental setup parameters and further passed through a conventional MLP with a number of hidden layers to the final prediction of an integral aerodynamic coefficient.

The input image of the configuration planform is propagated through a series of convolutional layers. A convolutional layer consists of a two-dimensional convolution followed by a max-pooling operation. The output after the max-pooling operation is passed through an activation function, where a leaky rectified linear unit (LeakyReLU) function serves system-wide as the used activation function [26, 27]. The activated layer output is further normalized by so-called layer normalization, which helps to reduce training time by normalizing the activities of the neurons within the network [28]. After the passing of all convolutional layers, the final output size $c_{out} \times w_{out} \times h_{out}$ is transformed into a vector size $(c_{out} \cdot w_{out} \cdot h_{out}) \times 1$, where c_{out} refers to the number of output channels and w_{out} & h_{out} refer to the output image dimensions.

In the following sequence, the flattened image vector is concatenated with a set of input features. These input features include the wind tunnel flow parameters Mach number M_∞ and Reynolds number Re , the aspect-ratio AR as additional geometrical input, the angle of attack α and angle of sideslip β as well as the control surface deflections η_{levcon} , ϵ_{slats} and δ_{flaps} . It shall be noted that the current configurations only feature deflections for levcon and slat devices (see section 2, Table 2 and Figure 5a). The input feature for trailing edge flap devices is added for maximum flexibility of the prediction model with respect to future aircraft configurations, which may include flaps as control surfaces.

The fully connected layer is further passed through a number of hidden layers, where again, each neuron is activated with the LeakyReLU function. In the final layer, all neurons are concentrated into the final output layer, where the integral aerodynamic coefficient is predicted.

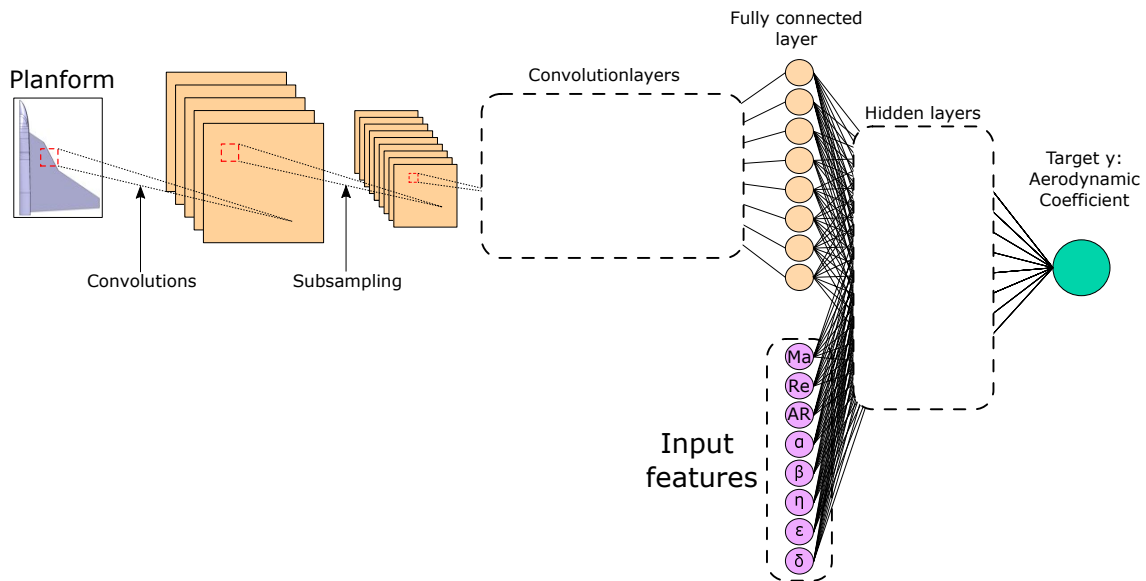


Figure 4: Schematic architecture of the proposed hybrid neural network (HNN).

3.2 Hyperparameter Optimization

The fine-tuning of the HNN is performed by a hyperparameter optimization with the *Optuna* framework [29]. *Optuna* is a *define-by-run* optimization framework, particularly developed for hyperparameter optimization of neural networks. Additionally, key elements of the software are the efficient implementation and the versatile architecture, which enables an easy setup of the optimization runs. *Optuna* implements a Tree-structured Parzen Estimator (TPE) algorithm with an additional pruning mechanism. Pruning itself can be seen as an early-stopping method, where the algorithm detects automatically if the current trial shows promising results compared to a set of earlier trials or if the current trial should be canceled and another trial with a new set of hyperparameters should be started [29].

The optimization run covered a total number of 250 trials, where 192 trials were pruned early. In Table 3, the most important hyperparameters of the HNN are listed.

Table 3: Overview of HNN hyperparameters.

Hyperparameter	
Initial learning rate	0.001
Batch size	16
Convolutional layers	3
Number of conv channels	10
Dimension of hidden layers	135
Hidden layers	14

3.3 Data Preprocessing

To enable future flexibility with respect to different configurations or datasets, a preprocessing step is necessary before starting the training algorithm. In particular, all experimental data needs to be combined in one uniform spreadsheet. In Table 4, the header of this spreadsheet is depicted. This simplicity enables the user to easily add other configurations at various flow conditions to further expand the capabilities of the prediction tool. Additionally, for each configuration, an image of the wing planform is needed to be saved within the spreadsheet. This image should be in the *Portable Network Graphics*-format. Due to memory and performance concerns, the image resolution or pixel size will be scaled to 256×384 pixels before passing it to the HNN. In Figure 5a, a sample of a wing planform is shown. Additionally, the levcon and slat control surfaces, corresponding to η_{levcon} and ε_{slats} in Table 4, are marked. In Figures 5b and 5c, the deflected control surfaces on the physical model are shown.

Table 4: Preprocessed training data spreadsheet.

config	M_∞	Re	AR	α	β	η_{levcon}	ε_{slats}	δ_{flaps}	C_L	C_m
\vdots	\vdots	\vdots	\vdots	\vdots	\vdots	\vdots	\vdots	\vdots	\vdots	\vdots

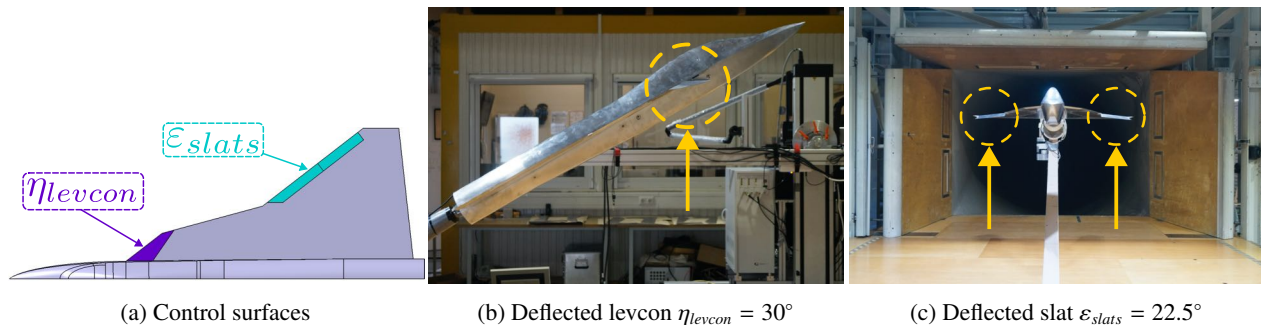


Figure 5: Control surface definitions.

3.4 Training of the Neural Network

Prior to the training, four configuration and their respective datasets are excluded from the total training process. These four configurations will serve as testing datasets, where the results will be shown in section 4. Further, the remaining dataset is split into a training and a validation set, where 80% of the data will be used for training and 20% will be used as validation and monitoring data. Additionally, the so-called dropout technique is employed during the training process of the network [30]. Dropout prevents units in a neural network from co-adapting too much, which as a result, prevents overfitting. The key idea is to randomly drop neurons and their connections from the neural network during training time, wherein the current case, the dropout rate is set to $p = 0.25$.

By monitoring the losses during the training process, an early stopping method in combination with a so-called learning rate scheduler can be applied. The algorithm detects plateaus of the validation loss during training. If the validation loss does not reach a new minimum value within a predefined number of patience epochs, the learning rate is adjusted by $lr_{new} = 0.1 \cdot lr_{old}$. A minimal learning rate of $lr_{min} = 10^{-6}$ is defined. In case the new learning rate does not result in a further reduction in the validation loss and the minimal learning rate is reached, the early stopping method will

PREDICTION OF AERODYNAMIC COEFFICIENTS

terminate the training process before reaching the maximum number of training epochs.

The mean squared error (MSE) per epoch is defined as the sum of the mean squared error per batch divided by the total number of batches (Equation 1). In Figure 6, the convergence of the training and validation losses for a different number of early stopping patience epochs are shown.

Figure 6a with patience = 0 epochs is already terminated after 8 epochs, where no convergence and proper training of the neural network is shown. A set patience of 10 epochs converges steadily towards a MSE of 10^{-4} and is terminated at ≈ 180 epochs before entering a training state of overfitting, where the neural network is adapting to the training data without improving on the randomly selected validation set. This behavior of overfitting can be seen in Figures 6c - 6f, where the training and validation losses are separating from each other and the validation loss stagnates at a level whereas the training loss further decreases with increasing epochs. As a result of this convergence study, the optimal number of patience epochs has been defined as 10 for the lift coefficient prediction. Following the same analysis and study, the training processes for the pitching moment coefficient predictions have shown an optimal number of 30 patience epochs.

$$MSE = \frac{\sum_{i=0}^{n.o.b.} MSE_{batch}}{n.o.b.}, \quad n.o.b. \hat{=} \text{number of batches} \quad (1)$$

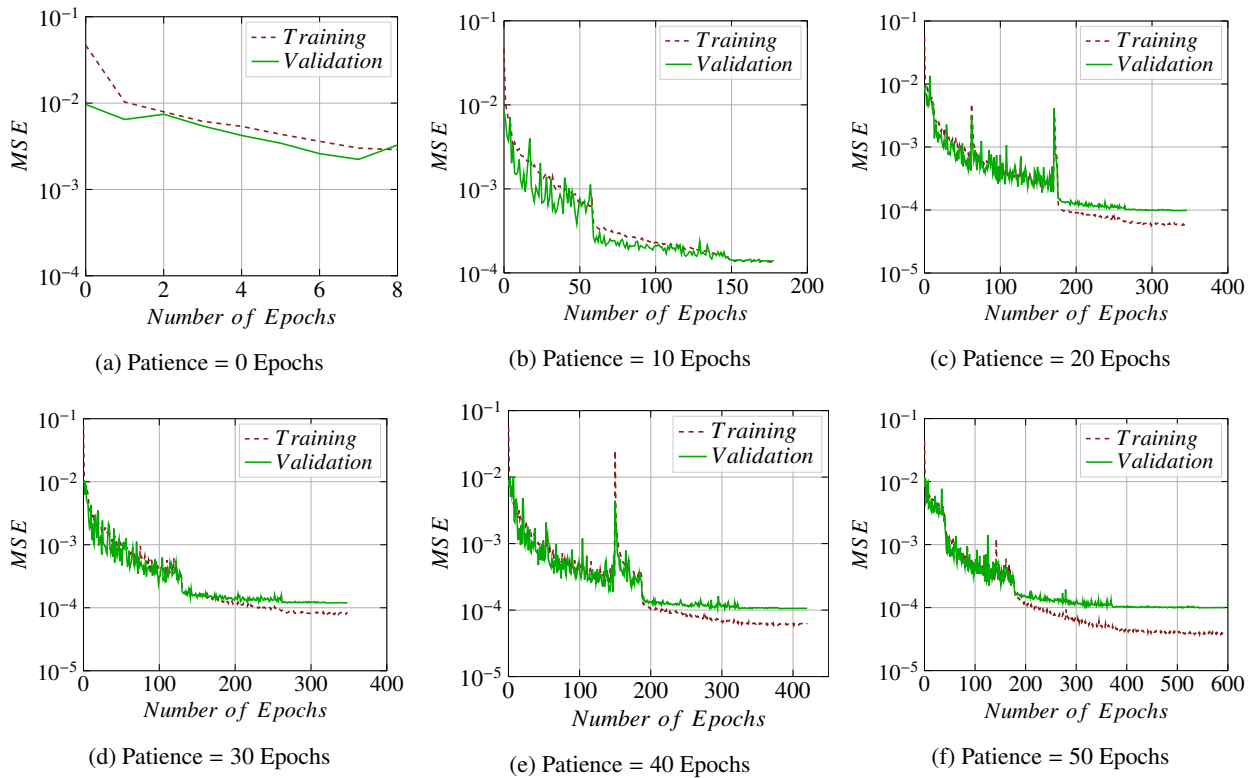


Figure 6: Convergence trends of training and validation losses with different learning rate scheduler patience epochs.

4. Results

In the following subsections, the results of the prediction of different aerodynamic coefficients for the previously introduced delta wing configurations will be discussed. In Figure 7, the training and validation losses for lift coefficient C_L in Figure 7a and the pitching moment coefficient C_m in Figure 7b are shown.

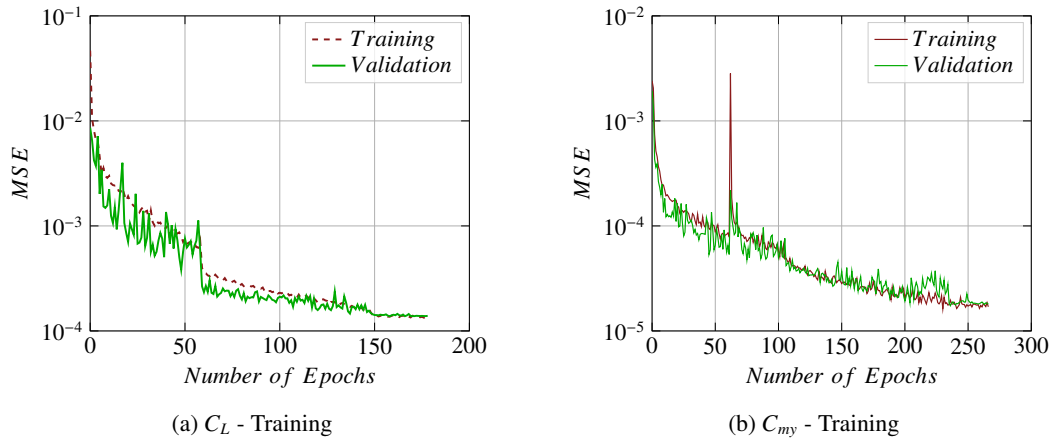


Figure 7: Mean squared error over number of training epochs.

4.1 Double Delta Wing - F2 xx7052 STLong

In the following, the results of aerodynamic coefficient predictions for an exemplary double delta wing configuration are presented. The F2 xx7052 STLong configuration and its geometric properties are shown in Figure 8. The configuration embodies a long strake section, $l_2/c_r = 0.35$ as described in Table 1, with a strake sweep angle of $\varphi_2 = 70^\circ$ and main wing sweep angle of $\varphi_1 = 52.5^\circ$. The resulting coefficient slopes will always be presented for an angle of sideslip $\beta = 0^\circ$ on the left-hand side and for $\beta = 5^\circ$ on the right-hand side, respectively. Experimental validation results, as described in section 2.3, are depicted as dotted lines with indication markers at the experimental data points. Additionally, the corresponding derivatives of the aerodynamic coefficients are plotted below the initial aerodynamic coefficient plot. It shall be noted that the primary focus lies on the prediction capability of the introduced hybrid neural network. A detailed discussion on the aerodynamic behavior and characteristics can be found in the publications of Pfnür et al. [17, 18].

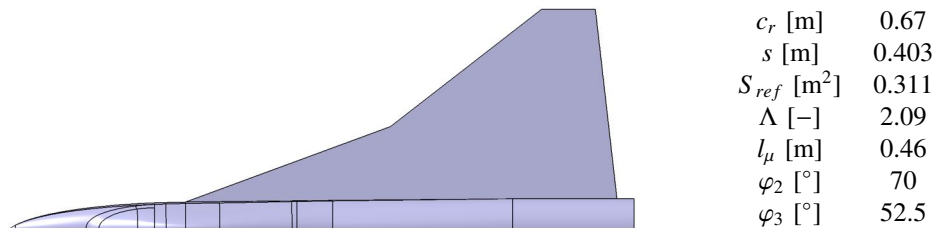


Figure 8: Double delta wing F2 xx7052 STLong configuration.

In Figure 9, the HNN lift coefficient predictions show very good agreement when compared to experimental data. The predicted slope for no control surface deflection $\varepsilon = 0^\circ$, $\eta = 0^\circ$ at $\beta = 0^\circ$ shows some minor deviation in the angle of attack range between $\alpha = 4^\circ - 20^\circ$, which is also represented in the slope of $C_{L\alpha}$. Additionally, the experimental outlier at $\alpha = 28^\circ$ also affects the prediction accuracy of $C_{L\alpha}$ in that region. The HNN predicted slopes for an employed slat deflection $\varepsilon = 22.5^\circ$, $\eta = 0^\circ$ represent experimental data very accurately with only small variances for low to moderate angle of attack regions. Whereas the left-hand slopes show excellent agreement in the highly non-linear region of $\alpha = 30^\circ - 40^\circ$, the right-hand slopes at $\beta = 5^\circ$ show some deviations up to the magnitude of $\approx 10\%$. Moreover, it can be seen that although trends in the slopes of $C_{L\alpha}$ can be predicted, absolute values can not be reproduced perfectly.

In Figure 10, the corresponding pitching moment coefficients are shown. Only the prediction at $\beta = 0^\circ$ with slat deflection shows good agreement with experimental results, especially below $\alpha = 20^\circ$. On the one hand, the prediction for the undeflected slat $\varepsilon = 0^\circ$ at $\beta = 0^\circ$ shows problems to reproduce the nose-down pitching moment for low angles of attack and both predicted slopes for $\beta = 5^\circ$ underestimate the pitching moment coefficient as a whole. On the other hand, if one compares the $C_{m\alpha}$ slopes in Figure 10, it can be seen that the characteristic trends are reproduced very well, where also absolute values match fairly well with experimental datasets. This comparison shows that although the

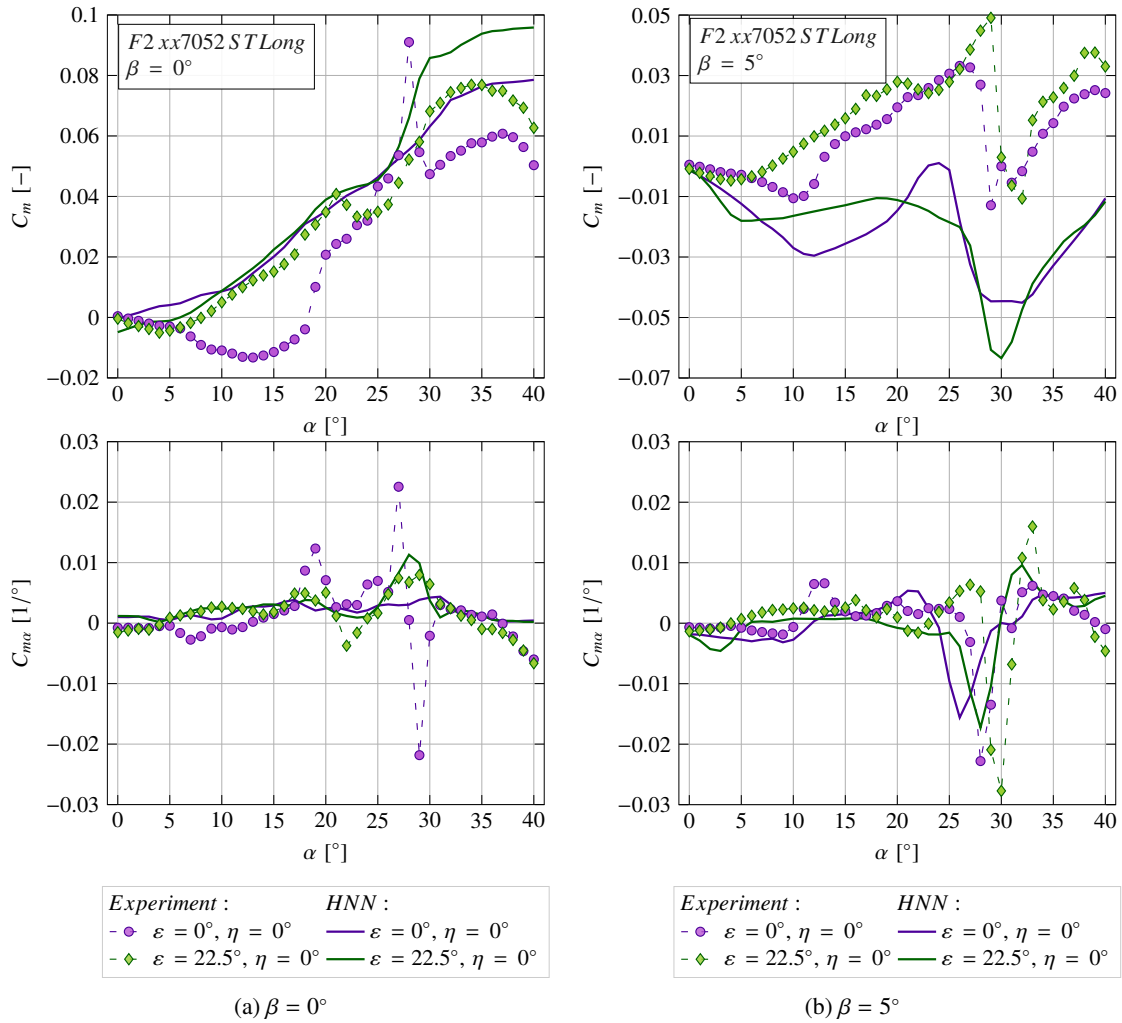


Figure 10: Pitching moment coefficient and corresponding derivative predictions of the F2 xx7052 STLong configuration.

4.2 Triple Delta Wing - F3 527052 STLong

In section 4.2, the results for the triple delta wing F3 527052 STLong configuration are presented. The wing planform and geometric properties are shown in Figure 11. The configuration embodies a levcon sweep angle of $\varphi_1 = 52.5^\circ$, again a long strake section, $l_2/c_r = 0.35$, with a strake sweep angle of $\varphi_2 = 70^\circ$ and main wing sweep angle of $\varphi_1 = 52.5^\circ$. Figures 12 and 13 show four HNN predicted slopes and four experimental datasets per angle of sideslip each. Single slopes correspond to certain control surface deflections, which are marked in the legends below the plots.

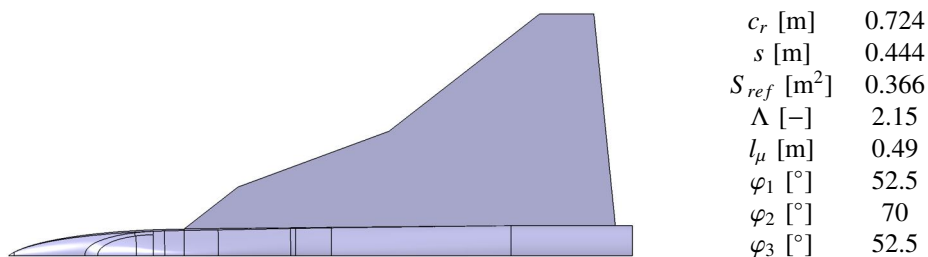


Figure 11: Triple delta wing F3 527052 STLong configuration.

PREDICTION OF AERODYNAMIC COEFFICIENTS

The HNN predicted lift coefficient slopes in Figure 12 altogether show a very good representation of experimental slopes, with deviations below 15%. This reproducibility is also depicted in the derivative $C_{L\alpha}$, where it can be seen not only aerodynamic characteristics but also absolute values are fairly well matched over the whole angle-of-attack range.

In contrast to the lack of accuracy of the pitching moment coefficient predictions for the double delta wing (Figure 10), the good agreement of prediction data with experimental data for the moderately swept triple delta wing F3 527052 STLong continues, when comparing slopes in Figure 13.

Trends and absolute values of HNN predicted C_m and $C_{m\alpha}$ are matched fairly well for both angles of sideslip and all kinds of control surface deflections. The predicted derivative $C_{m\alpha}$ shows some bigger deviations at high angles of attack, especially for the slope of $\varepsilon = 0^\circ$, $\eta = 30^\circ$ in Figure 13a, but overall the hybrid neural network shows great prediction capability for this type of configuration.

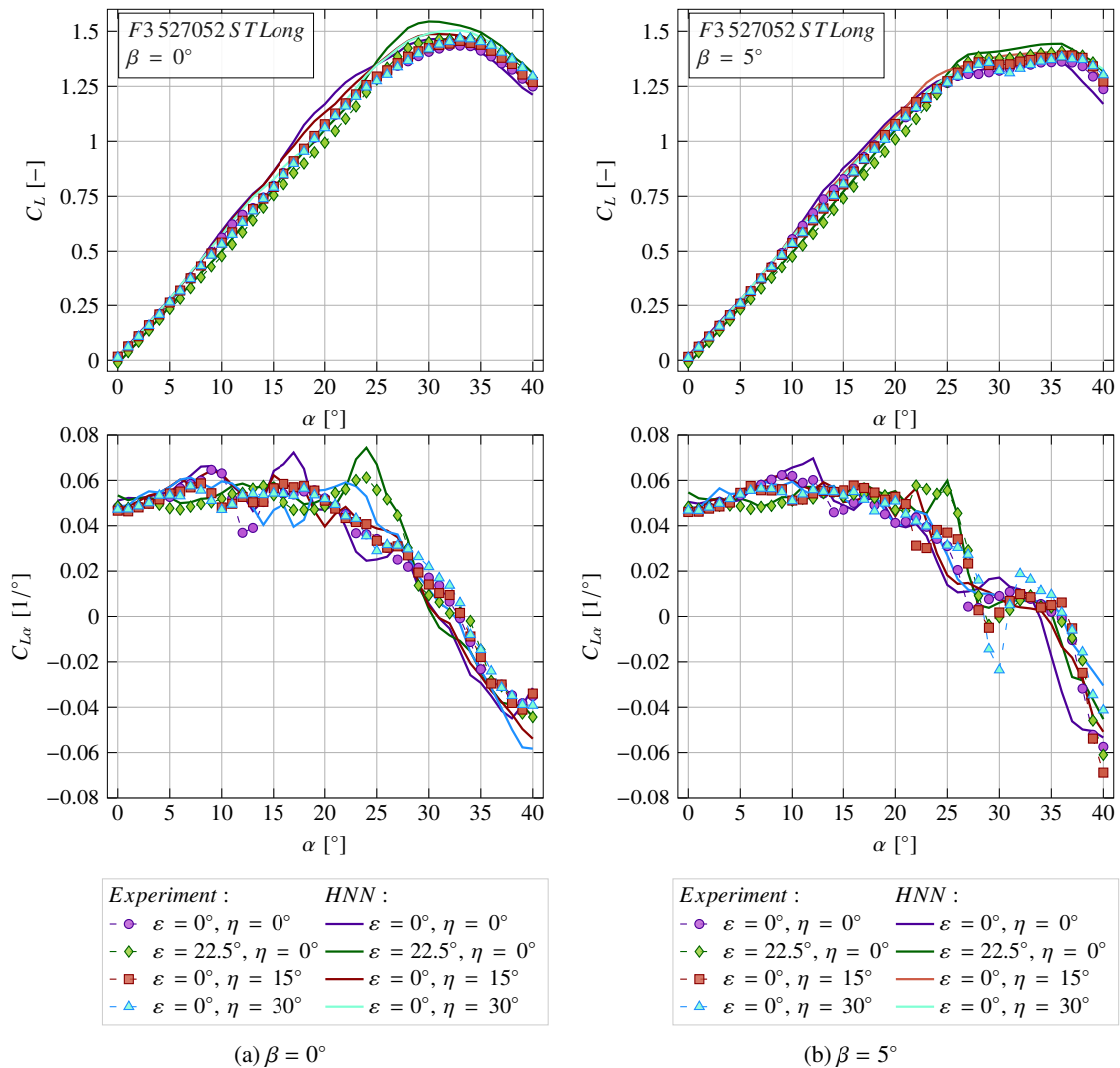


Figure 12: Lift coefficient and corresponding derivative predictions of the F3 527052 STLong configuration.

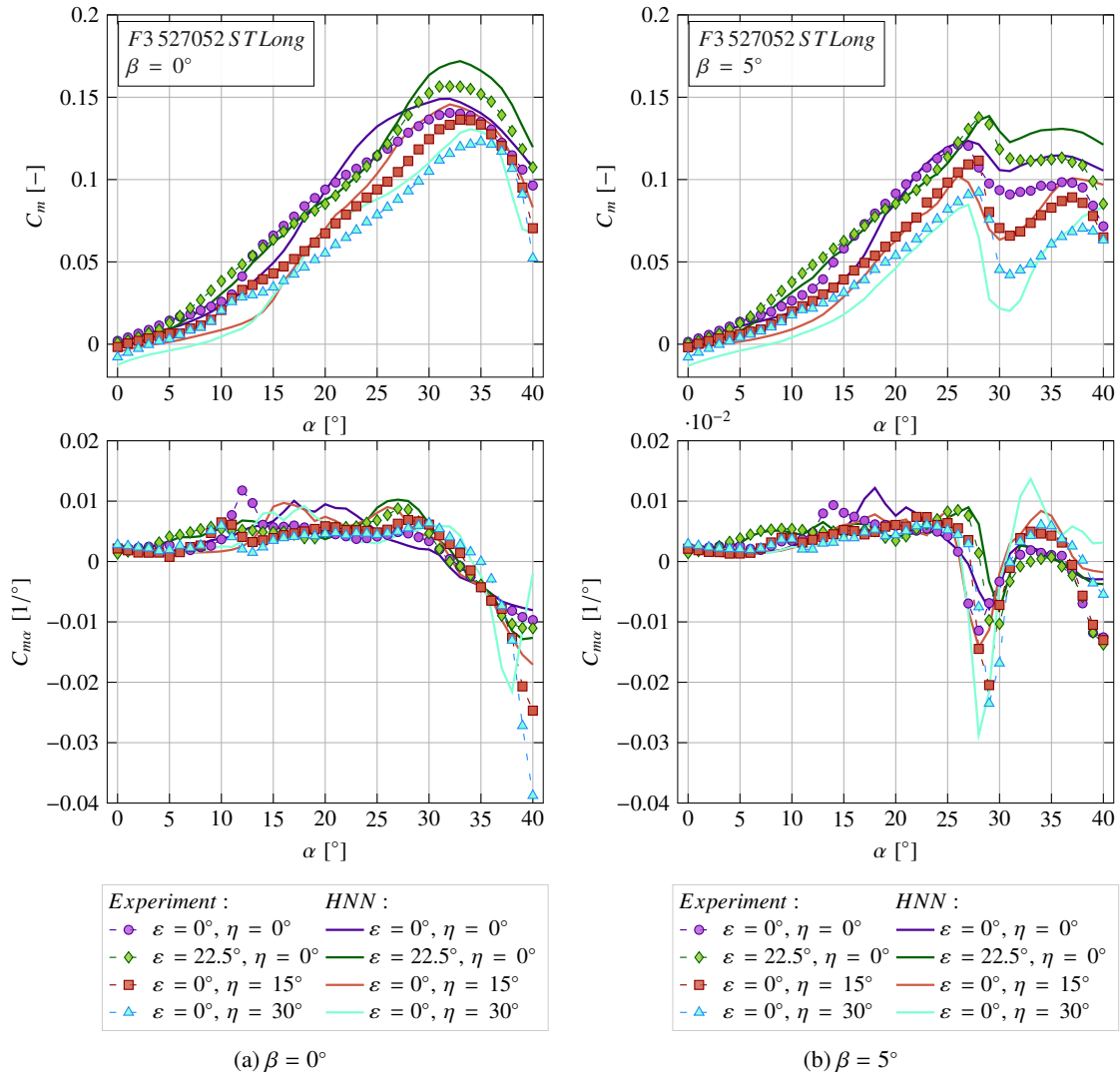


Figure 13: Pitching moment coefficient and corresponding derivative predictions of the F3 527052 STLong configuration.

4.3 Triple Delta Wing - F3 607560 STShort

In section 4.3, the results for the triple delta wing F3 607560 STShort configuration are presented. The wing planform with its main geometric properties are shown in Figure 14. The configuration embodies a levcou sweep angle of $\varphi_1 = 60^\circ$, and a short version of the strake section with $l_2/c_r = 0.25$ with a sweep angle of $\varphi_2 = 75^\circ$ and main wing sweep angle of $\varphi_1 = 60^\circ$.

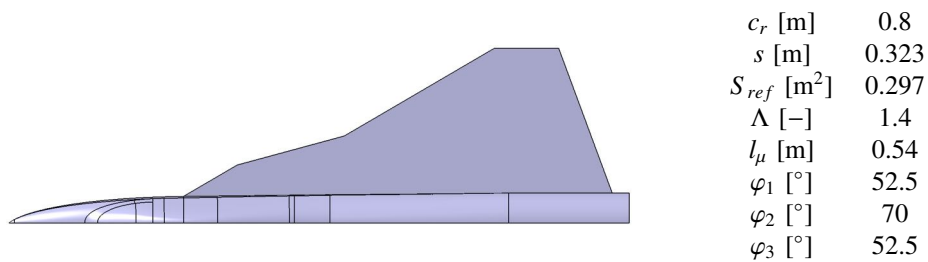


Figure 14: Triple delta wing F3 607560 STShort configuration.

PREDICTION OF AERODYNAMIC COEFFICIENTS

As for the triple delta wing in section 4.2, Figures 15 and 16 show four HNN predicted slopes and four experimental datasets at different control surface deflections per angle of sideslip each.

Results for the lift coefficient C_L predictions and its derivative $C_{L\alpha}$ show a more or less perfect match up to high angles of attack in comparison to experimental data. Pitching moment coefficient slopes in Figure 16 are also well predicted for low and moderate angles of attack. At higher angles of attack, the deviations from the HNN with respect to the experimental data increase to approximately 15 – 25%, which is still in good agreement. Further, the aerodynamic trends and characteristics are still preserved.

Looking at the HNN predicted slopes of $C_{m\alpha}$, the results at $\beta = 0^\circ$ in Figure 16a show well-matched trends and only bigger variances at high angles of attack. Especially the predicted slopes at $\beta = 5^\circ$ in Figure 16b show larger deviations at higher angles of attack $\alpha > 30^\circ$ in comparison to experimental results.

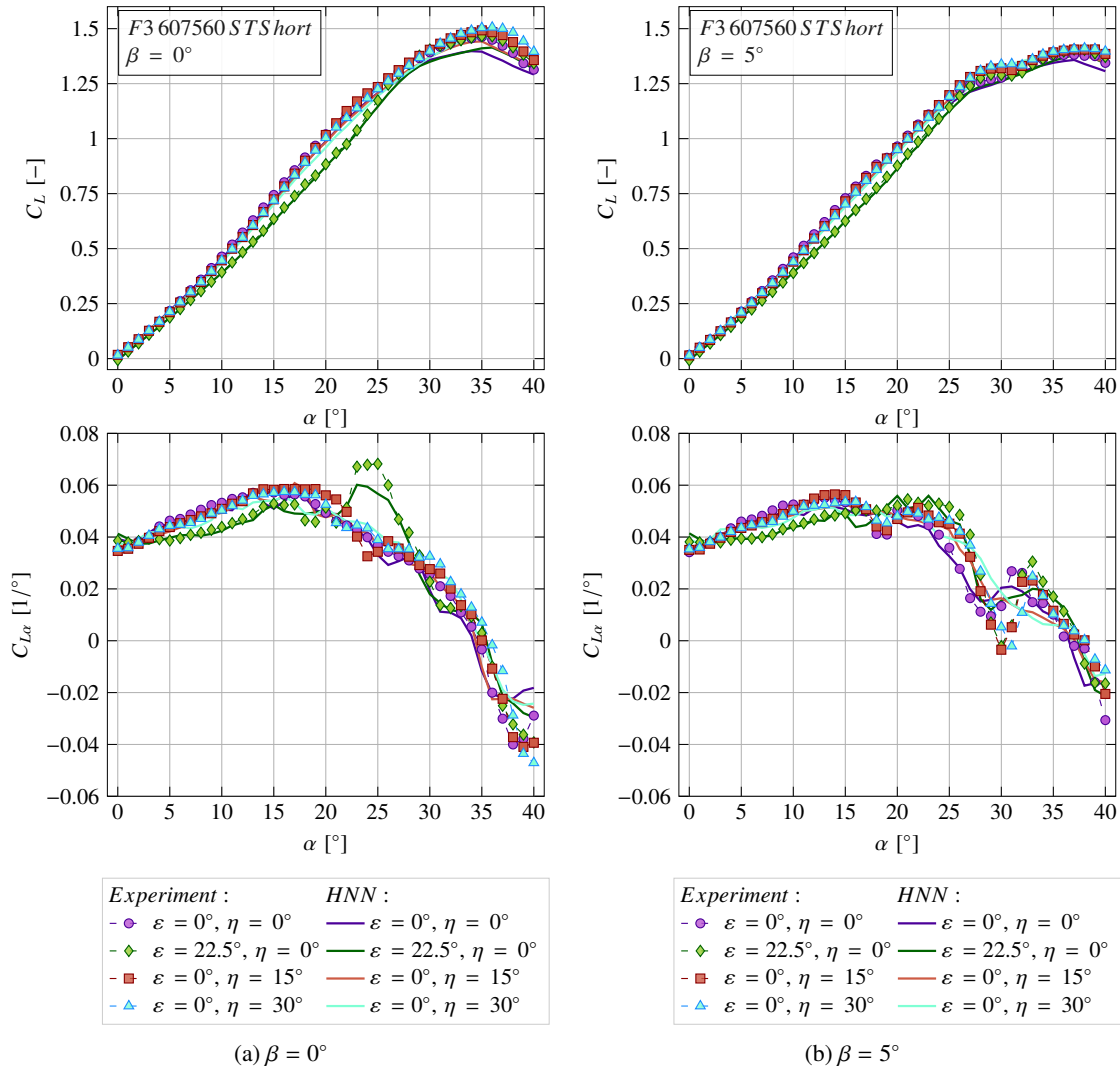


Figure 15: Lift coefficient and corresponding derivative predictions of the F3 607560 STShort configuration.

5. Error Quantification

The presented coefficient slopes in section 4 show that the introduced HNN is capable of predicting aerodynamic coefficients for unknown multiple swept delta wing configurations. In the angle-of-attack range of $\alpha = 0^\circ - 40^\circ$, the maximum deviation of the HNN predicted lift coefficient is below 15% for all possible control surface deflection and angle of sideslip combinations. If data is considered only for the range of $\alpha = 20^\circ - 40^\circ$, the predicted lift coefficients are all within a 10% range compared to experimental data, which is considered as a very good agreement.

Overall error quantification for the predictions of pitching moment coefficients is more difficult since, at very small

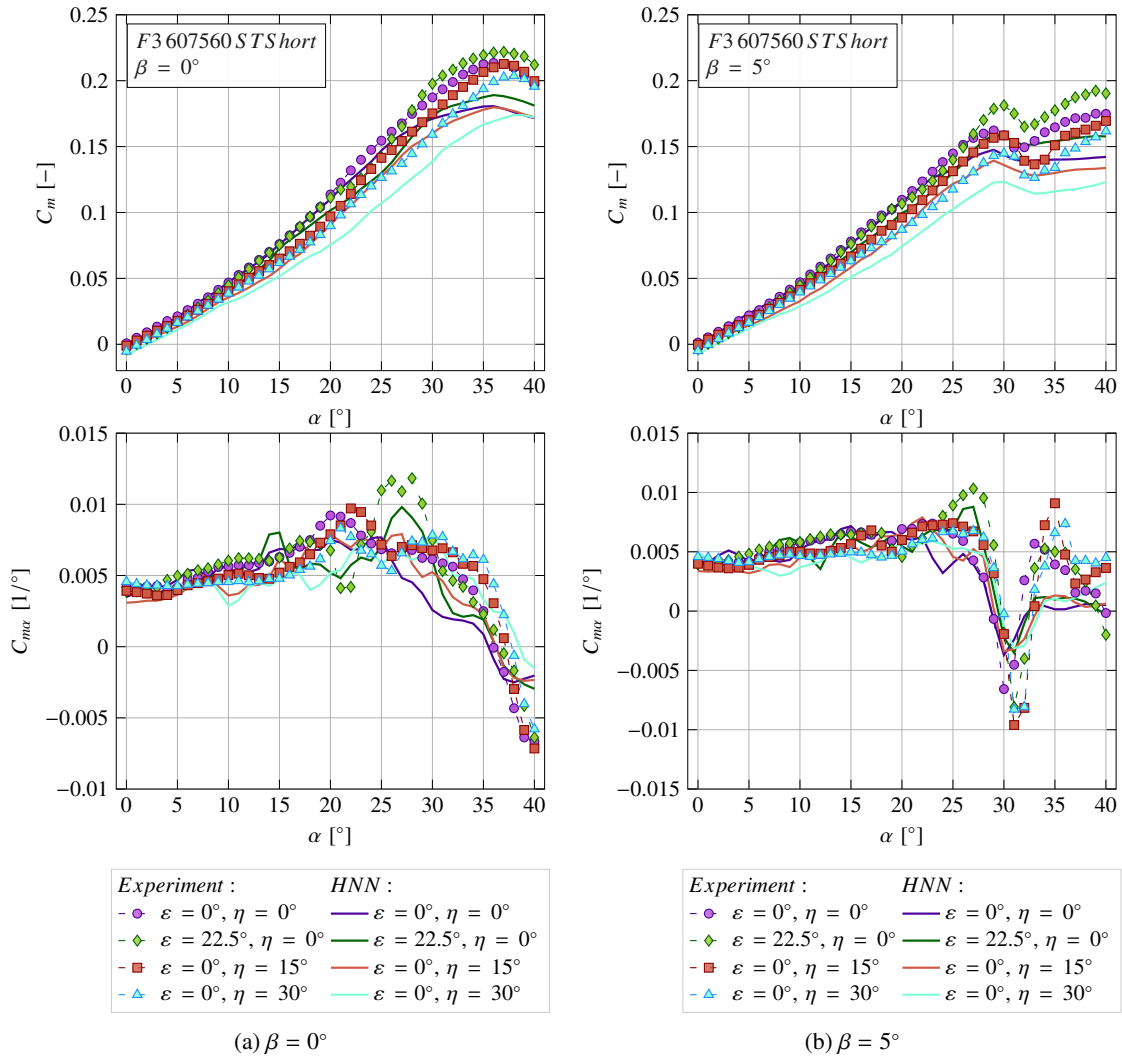


Figure 16: Pitching moment coefficient and corresponding derivative predictions of the F3 607560 STShort configuration.

numbers, deviations can quickly show high percentage-wise errors. If, for example, an experimental value of $C_{m,exp} = 0.05$ is compared to a predicted coefficient of $C_{m,pred} = 0.025$, the error is at 50% although the absolute error may be very small. Additionally, since especially the range of moderate to high angles of attack is of great interest for these types of configurations, only data for $\alpha = 20^\circ - 40^\circ$ is considered in the pitching moment coefficient error quantification.

On the one hand, as shown in Figure 10, the HNN predictions show great discrepancies for the pitching moment coefficient of the double delta wing configuration in comparison to wind tunnel data, which is especially obvious for the angle of sideslip of $\beta = 5^\circ$ in Figure 10b. On the other hand, the pitching moment coefficient can be predicted very well for both triple delta wing configurations presented in sections 4.2 and 4.3. For the F3 527052 STLong configuration in section 4.2, the maximum deviation of all considered pitching moment coefficients are below 60% in comparison to experimental data and are still considered well predicted when objectively analyzing the coefficient slopes. The predicted pitching moments for the F3 607560 STShort configuration presented in Figure 16 show a maximum deviation of 25%, which is considered a very good agreement with respect to experimental data.

6. Conclusion

The prediction capabilities of a hybrid neural network with respect to the prediction of aerodynamic coefficients and their characteristic slopes over a wide range of angles of attack for multiple swept delta wing configurations have been investigated. Experimental wind tunnel results of generic double and triple delta wing configurations served as underlying

PREDICTION OF AERODYNAMIC COEFFICIENTS

ing training, validation and test datasets. These generic wing planforms embody a wide range of different leading-edge sweeps and cover a wide range of different low aspect-ratio delta wing configurations.

The final test dataset has been excluded from the training data to fully analyze the prediction performance of the trained neural network on totally new unseen datasets. The results show that especially the lift coefficient C_L can be predicted with high accuracy in the whole angle-of-attack range for both triple and double delta wings. The aerodynamic characteristics associated with the derivative $C_{L\alpha}$ can also be reproduced fairly well. But it has to be noted that although characteristics and trends are predicted well, absolute values of derivatives can differ significantly from experimental values.

Whereas the neural networks show a problem at the prediction of the pitching moment coefficient C_m for a double delta wing configuration, it reproduces C_m and its characteristic $C_{m\alpha}$ with very high accuracy for both presented triple delta wings.

With the addition of experimental datasets of other delta wing configurations, exceeding the currently used generic platform, also at different Mach numbers M_∞ , the prediction capabilities and flexibility of the presented neural network are further improved. Fast and accurate predictions of coefficient slopes and aerodynamic characteristics could be beneficial tools in the preliminary aircraft design phase.

7. Acknowledgments

The funding of the presented work within the Luftfahrtforschungsprogramm VI-1 (LUFO VI-1) project DIGIfly (FKZ: 20X19091) by the German Federal Ministry for Economic Affairs and Climate Action (BMWK) is gratefully acknowledged.

References

- [1] Hitzel, S.: Sub- and transonic vortex breakdown flight condition simulations of the F-16XL aircraft. *Journal of Aircraft* **54**(2), 428–443 (2017). <https://doi.org/10.2514/1.c033246>
- [2] Hummel, D.: On the vortex formation over a slender wing at large angles of incidence, vol. AGARD CP-247 (1978)
- [3] Kohlman, D.L., Wentz, W.H.: Wind tunnel investigations of vortex breakdown on slender sharp edged wings, vol. NASA CR-98737 (1968)
- [4] Lambourne, N.C., Bryer, D.W. ARC-22775. H.M. Stationery Office (1961). <https://books.google.de/books?id=GIXzMgEACAAJ>
- [5] Polhamus, E.C.: Applying slender wing benefits to military aircraft. *Journal of Aircraft* **21**(8), 545–559 (1984). <https://doi.org/10.2514/3.45023>
- [6] Breitsamter, C.: Unsteady flow phenomena associated with leading-edge vortices **44**(1), 48–65. <https://doi.org/10.1016/j.paerosci.2007.10.002>
- [7] Duraisamy, K., Iaccarino, G., Xiao, H.: Turbulence modeling in the age of data **51**(1), 357–377 (2018). <https://doi.org/10.1146/annurev-fluid-010518-040547>
- [8] LeCun, Y., Bengio, Y., Hinton, G.: Deep learning **521**(7553), 436–444. <https://doi.org/10.1038/nature14539>
- [9] Zhang, Y., Sung, W.J., Mavris, D.N.: Application of convolutional neural network to predict airfoil lift coefficient. In: 2018 AIAA/ASCE/AHS/ASC Structures, Structural Dynamics, and Materials Conference. American Institute of Aeronautics and Astronautics. <https://doi.org/10.2514/6.2018-1903>
- [10] Suresh, S., Omkar, S.N., Mani, V., Prakash, T.N.G.: Lift coefficient prediction at high angle of attack using recurrent neural network. *Aerospace Science and Technology* **7**(8), 595–602 (2003). [https://doi.org/10.1016/s1270-9638\(03\)00053-1](https://doi.org/10.1016/s1270-9638(03)00053-1)
- [11] Nørgaard, M., Jorgensen, C., Ross, J.: Neural network prediction of new aircraft design coefficients." NASA TM-112197 (1997)
- [12] Meade, A., J. A.: An application of artificial neural networks to experimental data approximation (1993)

- [13] Huang, S., Miller, L., Steck, J.: An exploratory application of neural networks to airfoil design. In: 32nd Aerospace Sciences Meeting and Exhibit. American Institute of Aeronautics and Astronautics (1994). <https://doi.org/10.2514/6.1994-501>
- [14] Stradtner, M., Drazen, D., van Rooij, M.: Introduction to avt-351: Enhanced computational performance and stability & control prediction for nato military vehicles. In: AIAA SCITECH 2023 Forum. American Institute of Aeronautics and Astronautics (2023). <https://doi.org/10.2514/6.2023-0820>
- [15] Chaves, D.A.H., Bekemeyer, P.: Data-driven reduced order modeling for aerodynamic flow predictions. In: Ecomas Congress 2022 (2022). <https://elib.dlr.de/189313/>
- [16] Hitzel, S.M., Winkler, A., Hövelmann, A.: Vortex flow aerodynamic challenges in the design space for future fighter aircraft. In: Notes on Numerical Fluid Mechanics and Multidisciplinary Design, pp. 297–306. Springer (2019). https://doi.org/10.1007/978-3-030-25253-3_29
- [17] Pfnür, S., Breitsamter, C.: Leading-edge vortex interactions at a generic multiple swept-wing aircraft configuration **56**(6), 2093–2107 (2019). <https://doi.org/10.2514/1.c035491>
- [18] Pfnür, S., Pflüger, J., Breitsamter, C.: Analysis of vortex flow phenomena on generic delta wing planforms at subsonic speeds. In: Notes on Numerical Fluid Mechanics and Multidisciplinary Design, pp. 328–337. Springer (2019). https://doi.org/10.1007/978-3-030-25253-3_32
- [19] Hövelmann, A., Winkler, A., Hitzel, S.M., Richter, K., Werner, M.: Analysis of vortex flow phenomena on generic delta wing planforms at transonic speeds. In: Notes on Numerical Fluid Mechanics and Multidisciplinary Design, pp. 307–316. Springer (2019). https://doi.org/10.1007/978-3-030-25253-3_30
- [20] Sedlacek, D., Biechele, S., Breitsamter, C.: Numerical investigations of vortex formation on a generic multiple-swept-wing configuration **13**(1), 295–310. <https://doi.org/10.1007/s13272-021-00566-y>
- [21] Sedlacek, D., Breitsamter, C., Visonneau, M., Guilmineau, E., Wackers, J.: Assessment of hybrid delta wing vortex flow investigation – part i at subsonic conditions. In: AIAA SCITECH 2022 Forum. American Institute of Aeronautics and Astronautics. <https://doi.org/10.2514/6.2022-0565>
- [22] Sedlacek, D., Breitsamter, C.: Aerodynamic characteristics and topology of interfering vortex systems at hybrid delta wings. In: AIAA SCITECH 2022 Forum. American Institute of Aeronautics and Astronautics (2022). <https://doi.org/10.2514/6.2022-0026>
- [23] Yuan, Z., Jiang, Y., Li, J., Huang, H.: Hybrid-DNNs: Hybrid Deep Neural Networks for Mixed Inputs. arXiv. <https://doi.org/10.48550/ARXIV.2005.08419>
- [24] Yuan, Z., Jiang, Y., Huang, H., Li, J.: Reservoir productivity prediction based on a hybrid deep neural network. In: 82nd EAGE Annual Conference and Exhibition. European Association of Geoscientists & Engineers (2021). <https://doi.org/10.3997/2214-4609.202010851>
- [25] Lecun, Y., Bottou, L., Bengio, Y., Haffner, P.: Gradient-based learning applied to document recognition **86**(11), 2278–2324. <https://doi.org/10.1109/5.726791>
- [26] Glorot, X., Bordes, A., Bengio, Y.: Deep sparse rectifier neural networks, vol. 15 (2010)
- [27] Maas, A.L.: Rectifier nonlinearities improve neural network acoustic models
- [28] Ba, J.L., Kiros, J.R., Hinton, G.E.: Layer Normalization. arXiv (2016). <https://doi.org/10.48550/ARXIV.1607.06450>
- [29] Akiba, T., Sano, S., Yanase, T., Ohta, T., Koyama, M.: Optuna: A next-generation hyperparameter optimization framework. In: Proceedings of the 25rd ACM SIGKDD International Conference on Knowledge Discovery and Data Mining (2019)
- [30] Srivastava, N., Hinton, G., Krizhevsky, A., Sutskever, I., Salakhutdinov, R.: Dropout: A simple way to prevent neural networks from overfitting. *Journal of Machine Learning Research* **15**, 1929–1958 (2014)